NASA-CR-200270

Final Report

Ionospheric Plasma Outflow in Response to Transverse Ion Heating: Self-Consistent Macroscopic Treatment

Grant # NAGW-2903

P.I.: Dr. N. Singh

During the grant period starting July 1, 1994, our major effort has been on the following two problems:

1. Temporal behavior of heavy Oxygen ion outflow in response to a transverse heating event.
2. Continued effort on ion heating by lower hybrid waves.

We briefly describe here the research performed under these topics.

1. Temporal response of O^+ ions to a transverse heating event

Observations of superthermal O^+ ions from Dynamic Explorer 1 have shown both up-flowing and down-flowing populations. A more interesting observation from AKEBONO satellite is that a cold ($< 1\ eV$) population of O^+ ions is commonly found at altitudes of several thousands of kilometers. Knowing that the O^+ ions originate in the ionosphere where they are generally cold ($< 1\ eV$) and gravitationally bound, the occurrence of cold O^+ ions at high altitudes is a mystery. Our recent modeling efforts [*Singh*, 1995] explain that the creation of the superthermal up- and down-flowing ions along with the generation of cold O^+ ions at high altitudes are all related phenomenon. Using a mesoscale particle-in-cell code, we investigated the time-dependent flow of O^+ ions in response to a brief (a few minutes) transverse heating event at altitudes of about 2000 *km*. The heating was chosen to produce ions up to about $15\ eV$ in perpendicular

energy. As expected, the ions having energies $> 8\ eV$ escape, while those with lesser energies are gravitationally bound, but they rise to high altitudes depending on their initial energy. Such ions become progressively colder as they move upward because their kinetic energy is converted into gravitational potential energy. Near the apex of their trajectory, the ions are quite cold. During their return journey downward, the ions are again accelerated to relatively large downward velocities as observed from the Dynamic Explorer.

The falling ions mirror upward when they reach the ionospheric altitudes. Thus the initially heated ions are trapped inside the flux tube and undergo a repeated bounce motion. Since initially ions have a wide range of perpendicular energies after the heating, the ions cover a wide range of altitude as they execute their bounce motions. The result of this bounce motion is that the ions become progressively colder with increasing altitude with the coldest ions occurring at the highest altitudes considered in the model.

The rising and falling superthermal ions and the very cold O^+ ions at high altitudes seen in the model have characteristics similar to those reported from observations from the Dynamic Explorer and AKEBONO satellites. The details of the models and results can be found in the publications enclosed along with this report.

2. Ion heating by lower hybrid waves

Lower hybrid waves are known to heat ions. In the auroral plasma lower hybrid waves are a part of the broadband VLF waves driven by auroral electron beams carrying both upward and downward currents. Normally the waves driven by the electron beams have wavelengths so long that they do not affect the ions. In other words, this implies that ions do not resonate directly with the fast waves driven by the electron beam. It has been suggested that lower hybrid waves evolve nonlinearly into short wavelength slow waves. When the waves have sufficiently evolved, they might resonate with the ions and heat them perpendicularly.

During the last six months we have attempted to simulate this nonlinear evolution on a computer. The computer model uses a 3-D PIC code, as demanded by the nature of the problem.

We have found that a sequential code cannot serve the purpose. This has led to develop a parallel code. The development of the parallel code is being continued now under a new grant (NAGW-4470).

Publications

1. N. Singh, Time response of O^+ to a weak transverse ion heating event in the polar ionosphere, *J. Geophys. Res.*, in press, 1995.
2. N. Singh, Fountain-like flow of heavy oxygen ions from the earth's ionosphere in response to transverse heating, *IEEE Trans. Plasma Science*, Special Issue on *Images in Plasma Science*, reviewed and resubmitted, Nov. 1995.

Time Response of O^+ to a Weak Transverse Ion Heating Event in the Polar Ionosphere

Nagendra Singh

Department of Electrical and Computer Engineering
University of Alabama
Huntsville, AL 35899

Submitted to *JGR*, May 17, 1995

Abstract:

Time response of O^+ ions to transverse ion heating in the polar ionosphere is studied by means of a particle code. Here we deal with relatively low levels of heating over a few minutes yielding superthermal ions energized up to a few *eV*. Under the influence of the upward mirror and downward gravitational forces, most of the heated ions are trapped between the topside ionosphere and some high altitude depending on their perpendicular energies. A few ions with sufficiently large perpendicular energy escape the gravitational pull, and the flux of such ions increases with the heating level. The trapped ions bounce back and forth. During the first upward transit of the heated ions, the transient outflux from the topside ionosphere is as large as 10^7 ions cm^{-2}/s and it subsequently decays to quite small values in a few tens of minutes. A large transient outflux ($\sim 3\times10^8$ ions cm^{-2}/s^{-1}) consisting of unheated ions develops even below the heating region lasting over just a few minutes. As the ions having relatively large energies continue their upward journey, and the less energetic ones begin to fall down, the O^+ drift velocity ranges from a relatively large negative value (downward) just above the dense O^+ plasma in the topside ionosphere to a large positive value at high altitudes. Substantial flux of downward moving ions is also seen. During subsequent upward motions, the bouncing ions form a well-defined, quite sharp expansion front. The bounce motion generates a succession of plateau formation over a period of several hours in response to a brief heating period of just a few minutes. This leads to nearly periodic oscillations in local densities, with the oscillation period increasing with altitude. In a time of about one day, the oscillations in the density cease due to the spatial dispersion of the heated ions having differing initial energies. Eventually the O^+ density profile becomes nearly stable, but remains extended with significantly enhanced O^+ density at high altitudes. A consequence of trapping of the ions by the downward gravitational force is that the kinetic energy of the ions decreases with the increasing altitude; the coldest ions appear near the top of apex of the trapped ion trajectory while the warmest ions appear near the bottom of the flux tube. Such cold ions are likely to contribute to the thermal O^+ population observed at altitudes of several thousand kilometers.

Introduction:

Transverse ion heating is a common feature of the Earth's magnetosphere. Such heating occurs over a wide range of altitude and latitude, and it is commonly invoked to explain the escape of gravitationally bound heavy ionospheric ions such as O^+ [*Lockwood et al*, 1985; *Li et al*, 1988; *Waite et al*, 1985]. In order to escape the Earth's gravity, O^+ ions in the topside ionosphere should be energized to about 10 *eV*. Escaping O^+ ions with energy in the range from a few hundreds of *eV* to several *keV* are commonly found at high altitudes in the auroral plasma. Such ions flow upward with conical pitch angle distributions, which are created when transversely heated ions are acted upon by the mirror force, and the cone angle progressively decreases with altitude. Such considerations for the measured energetic O^+ ions show that the heating must occur at a high altitude above about 5,000 *km*, where abundance of O^+ ions is normally too small to generate the observed large flux of about 10^9 ions $cm^{-2}\,s^{-1}$. Therefore, it is logical to ask how the gravitationally bound O^+ ions are transported to such high altitudes.

Barakat and Schunk [1983] suggested that enhanced electron temperature ($10^4 k$) can facilitate the escape of O^+ ions; the escape occurs by enhanced polarization electric fields. *Singh et al* [1989] showed that the enhanced electric field associated with the density gradients in the auroral cavity can lead to a relatively large O^+ flux. *Li et al* [1988] showed enhanced O^+ flux can be generated by raising parallel and/or perpendicular temperatures of O^+ ions at some low altitudes. Using isotropic hydrodynamic model, *Gombosi and Killeen* [1984] and *Schunk and Sojka* [1989] showed that the low altitude frictional heating leads to the upflow of O^+ ions. The frictional heating of O^+ ions and associated dynamics were treated by *Korosmezey et al* [1992] using a more sophisticated hydrodynamic model, in which temperature anisotropy was allowed. Recently *Wilson* [1994] pursued a similar idea using a semikinetic model. *Loranc and St. Maurice* [1994] also studied the temporal behavior of O^+ outflow in response to a fractional heating at altitudes below 500 *km* using a semianalytical kinetic model in which the polarization

electric field was assumed to remain uniform and constant. Since the frictional heating heats O^+ to about $\sim 1\ eV$, the heated ions do not escape; after an initial upflow the ions fall under the influence of the gravity [*Loranc and St. Maurice*, 1995].

The purpose of this study is to examine the dynamics of the non-escaping ions, which are energized to a few eV and remain gravitationally bound. Such ions show an interesting set of dynamical features, which have not been studied before. These features include (1) simultaneous occurrence of down-flowing O^+ below certain altitude, and up-flowing O^+ above it during the early phase of the evolution; (2) the down-flowing O^+ eventually bounce back and forth as they are trapped between the bottom of the flux tube and some high altitude depending on their initial kinetic energy; (3) when the trapped ions move upward, they create a plateau in the density; the leading edge of the plateau is like an expansion front, which moves with a nearly constant velocity; (4) recurring formation of the plateau is seen; this creates oscillation in local densities with a periodicity which increases with increasing altitudes from about 2 hours at a low altitude (geocentric distance $r = 10^4\ km$) to several hours at high altitudes, and (5) eventually the oscillations subside as the ions with different energy gains during the heating period disperse giving rise to an O^+ density distribution substantially extended in altitude compared to the one without the heating. The top of the extended distribution is near the apex of the trapped ion trajectory for the ion with the maximum initial energy. Due to the gravity, the kinetic energy of the trapped ions decreases with altitude producing very cold ions near the top of the density distribution.

Recently *Chandler* [1995] reported observations of the down flowing O^+. The downward velocity of the ions was typically $< 1 \cdot 5\ km/s$ below the altitude of $4000\ km$. Our simulation shows how a brief transverse ion heating leads to the creation of a population of falling ions during the very early phase of the bounce motion. The evolution of the falling ions from the initially upflowing population of heated ions is critically examined. In connection with the cleft ion fountain [*Lockwood and Horwitz*, 1985], *Horwitz* [1984] and *Horwitz and Lockwood* [1985] studied 2-dimensional trajectories of bouncing O^+ superthermal ions. They found a "hopping"

trajectory in $r-\lambda$ plane where r is the geocentric distance and λ is the latitudinal angle. The conversion of bounce motion into a hopping trajectory is caused by the $\underline{E}\times\underline{B}$ drift where $\underline{E}$ is the convection electric field. In the present paper, we have not included the convection field, as our main goal is to understand the basic dynamical features driven by the brief period of transverse ion heating. We report here the time constants of the different phases of the evolution from ion heating to the generation of extended O^+ density profiles. We also report here both the downflux and upward flux of O^+ ions generated by the transient heating and compare the latter with those produced in the steady-state models. The temporal and spatial evolutions of the fluxes are discussed.

Using data from the Akebono satellite, [*Abe et al*, 1993; *Peterson et al* 1993] reported a common occurrence of a stationary, dense cold O^+ population extending to altitudes of several thousand kilometers. How such cold O^+ ions are transported to such high altitudes has remained a mystery. We demonstrate here that the gravity in combination with transverse ion heating at low altitudes producing superthermal O^+ ions creates a cold O^+ population extending to high altitudes as observed

The rest of the paper is organized as follows. In section 2 we briefly describe the model. In section 3, we discuss the dynamics of the superthermally heated ions by the process of transverse ion heating. O^+ fluxes associated with the up- and down-flowing ions are discussed in section 4. Conclusions and discussion are given in section 5.

2. Numerical Model

We study plasma flow in an open flux tube as shown in Fig. 1. The topside ionospheric base is assumed to be at $r=r_b$. We simulate the flux tube up to a geocentric distance $r=r_{\max}$. We assume that Earth's magnetic field $B(r)\cong B_o(r_b)(r_b/r)^3$, where $B_o(r_b)$ is the magnetic field at $r=r_b$. In order to study the plasma flow, we employ a particle code [*Wilson et al*, 1990]. The model treats a collisionless plasma. Therefore, the boundary at $r=r_b$ is taken to be at a sufficiently high geocentric distance $r_b=7350\ km$ or altitude $h\cong 980\ km$. Note that in this

paper (height) $h = r - \mathrm{Re}$, where Re is the Earth's radius. We inject macroparticles corresponding to O^+ and H^+ ions into the flux tube at the boundary at $r = r_b$ and subsequently follow their dynamics under the influence of the gravity, polarization electric field and the mirror force associated with the gradient in the geomagnetic field. The injected particles are chosen from Maxwellian velocity distributions with a zero drift for O^+ and a non-zero drift for H^+. The choice of H^+ drift does not significantly affect the outflow of O^+ ions in response to the heating. In this paper we present results for a drift velocity of $1.55\, V_{tH}$, where V_{tH} is the thermal velocity corresponding to the temperature T_o of H^+ ions at the base. Only the charged particles with parallel velocity $V_{||} > 0$ are injected into the flux tube. We assume that O^+ and electron temperatures at $r = r_b$ are also T_o. When a steady-state polar wind flow is set up in the flux tube, we initiate the transverse heating event for O^+ ions. The heating is assumed to be extended and it occurs for all altitudes $h > 1940\ km$ $(r \geq 8311\ km)$. The heating at such altitudes is expected to be caused by wave-particle interactions in contrast to the frictional heating occurring at low altitudes discussed earlier. The heating occurs in a random fashion as described by *Brown et al* [1991]. Whether or not a particle is heated during a time step Δt depends on the probability density given by

$$p(\Delta w_\perp) = \frac{1}{2\pi\sigma} \exp\left[-\tfrac{1}{2}(\Delta w_\perp / \sigma)^2\right] \qquad (1)$$

where $\Delta w_\perp$ is the impulse of energy given to a O^+ macroparticle in the degree of freedom perpendicular to the magnetic field. In implementing this heating scheme, a random number R_n is chosen from a uniform distribution from 0 to 1 for each O^+ macroparticle lying in the desired altitude range. This number is compared against the cumulative probability associated with the above probability density and when the latter exceeds R_n, the energy of the particle is incremented by $\Delta w_\perp$. *Brown et al* [1991] showed that the above scheme gives a heating rate given by

$$\frac{\partial kT_\perp}{\partial t} \cong \sigma / 1.14\, \Delta t \qquad (2)$$

where Δt is the time step used in advancing the motion of the O^+ macroparticles, k is the Boltzmann constant, and $T_\perp$ is the average perpendicular temperature of the heated ions. Equation (2) defines σ in terms of the heating rate.

In our simulations we assumed that O^+ and H^+ densities at the base $r = r_b$ are $n_{O^+} = 0.9\, n_o$ and $n_{H^+} = 0.1\, n_o$, where n_o is the total plasma density there. At the base H^+ flow was assumed to be supersonic with an average flow velocity $u_{H^+}(r = r_b) = 1.55\, V_{tH}$, where $V_{tH} = \sqrt{kT_o / m_{H^+}}$ with m_{H^+} being the mass of an H^+. For O^+ we assumed $u_{O^+}(r = r_b) = 0$. Time step in advancing the motion of the macroparticles was $\Delta t = 11 s$. The polarization electric fields were calculated by assuming that electrons obey the Boltzmann law with a constant temperature T_o and the plasma remains quasineutral; this yields electric field $E = -(kT_o / e) \times n_e^{-1}\, \partial n_e / \partial x$, where $n_e = n_{O^+} + n_{H^+}$. In the following discussion we use the following definitions and normalizations: density $\bar{n} = n / n_o$, velocity $\bar{V} = V / V_{tH}$, electric field $\bar{E} = E / E_o$, and flux $\Gamma = \Gamma / \Gamma_o$ where n and V denote the density and velocity of charged particles, respectively; $\Gamma_o = n_o V_{tH}$, and $E_o = k_B T_o / eL$, with $L = V_{tH}^2 / g_o$, which is about $3000\, km$ for $T_o = 0.3\, eV$ and $g_o = 9.8\, ms^{-2}$ and $E_o = 1\, \mu V / m$. For the chosen parameters of our calculations ($n_o \cong 10^4\, cm^{-3}$ and $T_o = 0.3\, eV$) $V_{tH} \cong 5.5\, km / s$, $E_o = 1\, \mu V / m$ and $\Gamma_o = 5.5 \times 10^9\, ions\ cm^{-2}\, s^{-1}$.

3. Numerical Results

In this section we first briefly describe the ambient polar wind, followed by a detailed discussion on the transient outflow of O^+ ions, including interpretation of the numerical results.

3.1 Ambient Polar Wind

Starting with an empty flux tube, a polar wind consisting of O^+ and H^+ ions is set up by injecting charged particles into the flux tube at $r = r_b$ (Figure 1). It takes several hours to establish a stable polar wind as determined by the transit time of the slower O^+ ions, as they move upward and then fall under the influence of the gravity. Our numerical calculations showed that a

stable polar wind is set up in about 6 hours, which is roughly the time for O^+ ions with a velocity of $\sim 1\ km/s$ to travel from the boundary at $r = r_b$ to an altitude $r = 10^4\ km$ and then fall back to $r = r_b$. Figures 2a to 2f show the state of the ambient polar wind. Since the state shown in these figures serves as initial condition for further calculations on O^+ dynamics in response to transverse heating, we label this state by $t = 0$. Figures 2a and 2b show the phase space plots for O^+ ions in $r - V_\parallel$ and $r - V_\perp$ planes, respectively; $V_\parallel$ and $V_\perp$ are the components of velocity of charged particles parallel and perpendicular to the magnetic field. The corresponding plots for H^+ ions are in Figures 2c and 2d. O^+ ions are almost in static equilibrium, except for a few ions having initially large perpendicular velocities. These ions are propelled to relatively high altitudes under the influence of the mirror force. However, with the temperature $T_o = 0.3\ eV$ even these ions do not escape and are eventually turned downward. The O^+ phase space in $r - V_\parallel$ is quite symmetric about $V_\parallel = 0$ indicating an average drift velocity of zero.

Figure 2c shows that the light H^+ ions flow out and attain relatively large supersonic flow velocities all along the flux tube. Figure 2d shows the expected cooling in the perpendicular degree of freedom as H^+ ions move upward and eventually escape from the top of the flux tube.

The density profiles of the O^+ and H^+ ions in the ambient polar wind are shown in Figure 2e. The crossover point occurs at $r = 9100\ km$. This figure also shows the normalized polarization electric field $\bar{E}$ associated with the ambient polar wind. The maximum electric field occurs at the base $(r = r_b)$ and its volume is $E \cong 9.6\ E_o \cong 0.96\ \mu V/m$. The electric field profile is determined by the two density profiles in the figure because $E \propto n_e^{-1}\, \partial n_e / \partial x$ where $n_e = n_{O^+} + n_{H^+}$.

Profiles of the average flow velocities of O^+ and H^+ ions are shown in Figure 2f. For O^+ the average drift velocity is nearly zero all along the flux tube, as expected for a static equilibrium. On the other hand, H^+ ions are nearly supersonic all along the flux tube; near the base the average drift velocity is $1.55\, V_{tH}$. There is no net outflux of O^+ ions in the ambient polar wind. The outflux of H^+ ions is shown in the figure; we have plotted here $\bar{\Gamma}$ which is the normalized outflux defined by $\bar{\Gamma}(r) = \Gamma / n_o V_{tH} = \bar{n}_{H^+}(r)\, \bar{u}_{H^+}(r)\, (r/r_b)^3$. First of all we note that $\bar{\Gamma}(r)$

is nearly constant as a function of r, barring some fluctuation inherent to a PIC code. The constancy of $\overline{\Gamma}$ indicates that the code is fairly accurate. The constant value of $\overline{\Gamma}$ is determined by the boundary condition and it is $\overline{\Gamma} = 0.155$, which amounts to a flux $\Gamma = 0.155\, n_o V_{tH} \cong 8.5 \times 10^8$ *ions* $cm^{-2} s^{-1}$ at $r = r_b$. This flux is determined by the boundary conditions on H^+ average velocity ($1.55\, V_{tH}$) and density ($n_{H^+} = 0.1\, n_o$) at $r = r_b$.

3.2 Time Response to Transverse Heating

Our main goal here is to study the temporal behavior of transversely heated ions at relatively low altitudes. We consider here only a low level of heating which produces superthermal ions in a few eV energy range. We examine the temporal behavior of (a) the phase space in $r - V_{\parallel}$ and $r - V_{\perp}$ planes, (b) O^+ density and average flow velocity profiles and (c) temporal variation of the local ion densities. Figures 3a and 3b show the phase space plots after 5 minutes of heating with a heating rate $\partial / \partial t (kT_{\perp}) \cong 0.04\, kT_o / s$, which gives $\sigma = 0.5\, eV$ from equation (2). At this time we note that the perpendicular velocity distribution of the ions is significantly modified by the perpendicular acceleration of ions up to $V_{\perp} \cong 2.5\, V_{tH}$ and maximum perpendicular energy $W_{\perp \max} = 51\, kT_o$. Assuming $kT_o = 0.3\, eV$, $W_{\perp \max} \cong 15\, eV$.

For the flux tube we consider, any ion exiting from the top of the flux tube is essentially lost or escaped for our purposes. Ignoring parallel electric field, we can estimate the total energy required for such an escape and it is

$$W_{es} \approx - \int_{r=r_b}^{r=r_{\max}} g_o (\mathrm{Re}/r)^2\, dr \approx m_{O^+}\, g_o\, R_e^2 \left(\frac{1}{r_b} - \frac{1}{r_{\max}}\right) \qquad (3)$$

where g_o is the gravity at $r = \mathrm{Re}$, the Earth's radius.

For the parameters of our calculation ($r_b = 7350\ km$, $r_{\max} = 31350\ km$, $g_o = 9.8\ ms^{-2}$, $\mathrm{Re} = 6371\ km$), $W_{es} = 5.7\, eV$ or $19\, kT_o$. Therefore, we expect that heated ions with $V_{\perp} > (2\, W_{es} / m_{O^+})^{1/2} \cong 1.5\, V_{tH}$ will eventually escape from the flux tube. We point out that if the top boundary were taken to be at infinity, i.e., $r_{\max} \to \infty$, $W_{es} \cong 7.5\, eV$ and perpendicular escape velocity is then only slightly larger.

top boundary were taken to be at infinity, i.e., $r_{max} \to \infty$, $W_{cs} \cong 7.5\ eV$ and perpendicular escape velocity is then only slightly larger.

From the above consideration, we expect that some of the heated ions in Figure 3b will eventually escape from the flux tube as the mirror force accelerates them upward. On the other hand, those ions with $V_\perp < 1.5\, V_{tH}$ will be eventually returned downward after reaching their apex. This is clearly brought out from the phase space plots at later times as shown in Figures 3c and 3d for $t = 20$ min., Figures 3e and 3f for $t = 60$ min., and Figures 3g and 3h for $t = 120$ min. At $t = 20$ min., ions show parallel acceleration by the mirror force. When $t = 1$ hrs., the accelerated ions have reached the top of the simulated flux tube and their parallel average flow velocity is $u_{||} = 1.36\, V_{tH} = 7.4\ km/s$. Upflowing superthermal O^+ ions with this magnitude of parallel flow velocity have been observed from Dynamic Explorer 1 at geocentric attitudes shown in Figure 3 [*Waite et al*, 1985]. The phase space plots in Figure 3e shows that the average flow velocity of the upflowing ions varies almost linearly with the altitude. As the time passes, the heated ions having relatively low perpendicular energies begin to move down first. Figure 3g shows that at $t = 120$ min. ions are already falling ($V_{||} < 0$) at geocentric altitudes below $r < 18000\ km$, and the falling ions are beam-like until they begin to penetrate the dense O^+ population at low altitudes. Thus, for heights $h < 3000\ km$ ($r < 10{,}000\ km$) it is difficult to distinguish falling ions from the ambient O^+ population, but above this height falling O^+ create a distinct beam-like population and maximum downward velocity in the height range of about 4000 *km* is $|V_{||}| < 0.5\, V_{tH} \cong 2.5\ km/s$. At higher altitudes, the average downward flow velocity decreases with increasing height at $t = 120$ mins. At low altitudes below 4000 *km* also, the average flow velocity decreases and becomes quite small, as the falling ions penetrate into the dense O^+ population. This yields a maximum flow velocity somewhere in the midaltitude range. Recently *Chandler* [1995] reported data on downflowing O^+ form DE-1 satellite; his data are confined to altitudes <4000 km in the polar topside ionosphere. The data show that the downward flow velocity of O^+ nearly monotonically increases with altitude and reaches a value $\sim 2\ km/s$ at about 4000 *km* altitude. No observation is available on down flowing O^+ for

$h > 4000\ km$. Our simulation shows that average flow velocity of O^+ ions should monotonically decrease with distance above a certain altitude, where it maximizes, but the height of the maximum downward drift depends on the phase of the evolution. We further discuss this in a later section on O^+ flux.

The down-flowing O^+ event discussed above lasts for much longer time than that covered in Figure 3. Figure 4 shows the further evolution of the transversely heated ions including those flowing down. The downward flowing ions with flow velocity varying almost linearly with the altitude are seen in Figures 4a and 4c, which show the phase space plots in $r - V_{\parallel}$ plane for 4, and 6 hours, respectively. Such downflowing ions recede from the top and eventually disappear as seen from Figure 4e for $t = 8$ hrs. However, they reappear as shown for $t = 12$ hrs. when the down flowing ions mirror and move upward to fall again, as discussed below.

Beside falling O^+ ions, Figures 4a to 4h show another interesting feature of the O^+ dynamics in response to the brief heating lasting over 5 minutes. Figures 4a and 4b reveal that besides the bulk of O^+ below $r \cong 10^4\ km$, a band of new O^+ cloud is appearing at higher altitudes as indicated by an arrow in Figure 4a. This band of O^+ ions in $r - V_{\parallel}$ plane has a distinctive signature in the $r - V_{\perp}$ plane as well, as indicated by an arrow. Near the cloud the density in the phase space is relatively high as marked by the dense packing of the dots representing ions. Figures 4c and 4d for $t = 6$ hrs. show that the O^+ cloud in the band move upward, and a new band appears to separate from the dense O^+ plasma at the bottom. Figures 4e and 4f for $t = 8$ hrs. show that both bands of O^+ cloud appearing in Figures 4c and 4d have moved up. At later times the ions in the first band begin to fall after reaching their apex, while the ions in the second band continue to move up; these features are seen from Figures 4g and 4h for $t = 12$ hrs. These figures show the development of additional bands. The band structure appearing in the phase space plots of Figures 4a to 4h is a consequence of downflowing ions mirroring back and moving upward again. However, a question arises as to the cause for the more than one band to appear. The upward motion of the superthermal ions is self-modulating; as the ions move up modifying the density profile, the electric field is modulated in time. When the

in the electric field has an appreciable affect on the O^+ dynamics. This creates bunching of the superthermal ions; each bunch appears as a band in the $r - V_{\parallel}$ phase space. We will further discuss the oscillation in the electric field after presenting the dynamic behavior of O^+ density profile

Evolution of O^+ Density Profile: The repeated upward motion of the mirroring ions is more clearly seen by looking at the density and the average flow velocity profiles of O^+. Figure 5 shows the evolution of the O^+ density profile for times before $t = 3$ hrs., about the time when the mirroring ions begin to move upward for the first time after their first fall. For the purpose of comparison, we also give the O^+ density profile at $t = 0$ in the ambient polar wind. In response to the heating, O^+ ions move upward as they are accelerated upward by the mirror force, without any significant change in the flow of H^+ ions. By the time $t = 1$ hrs. the heated ions begin to reach the top of the simulated flux tube. As the heated upwelling ions disperse in the flux tube to higher and higher altitudes and some of them flow out from the top, the density beings to drop in the newly populated altitude region as seen from the plots for $t \geq 90$ min. The flux of O^+ in such an upwelling event will be discussed later. We notice from Figure 5 that at $t = 180$ min., the density profile beings to expand again as evidenced by the formation of a ledge in the density profile below $r = 14{,}000\ km$. This re-expansion is shown in Figure 6, which shows density profiles from $t = 3$ hrs. to 6 hrs. The re-expansion is accompanied by a well-defined expansion front as marked by arrows. The velocity of expansion front is nearly constant and it is about 600 *m/s*. Locations of the expansion fronts correspond to the previously discussed formation of the first band of O^+ cloud seen in the phase space plots in Figures 4a and 4c. The evolution of the average flow velocity of O^+ for the expanding plasma in Figures 6 is shown in Figure 7. Note that the velocities shown are normalized to $V_{dH} = 5.5\ km/s$. The location of the expansion front is where the velocity has a sharp jump from a small positive value to a relatively large negative value. The negative velocity above the locations of sharp jump corresponds to the falling ions, discussed earlier in connection with Figures 3 and 4. Thus, the expansion front separates the

upflowing ions just below it from the downflowing ions above it. Below the expansion front the average velocity is generally quite small and it approaches zero in the dense O^+ plasma at low altitudes. However, at times the downflowing ions may dominate even below the expansion front as revealed by the average flow velocity at $t = 6$ hrs. in Figure 7; at this time the average upward velocity near the expansion front is about $500\ m/s$, while just below it the average downward velocity is about $1\ km/s$. Figure 6 shows that at $t = 6$ hrs. there is yet another new expansion front separating from the dense plasma at low altitudes; the new expansion front corresponds to the new band appearing in the phase space in Figure 4c. Further expansion of this new front is shown in Figure 8 by the short arrows. We notice both the old and new expansion fronts in this figure; the new front is at lower altitudes, while the old one has traveled to $r \cong 2300\ km$ by $t = 8$ hrs, as indicated by the long arrows.

Electric Field Oscillations: The above dynamical behavior of the O^+ density modulates the electric field in time, which in turn affects the dynamics of the O^+ ions as they bounce back and forth. The inset of Figure 5 shows an example of oscillation in the electric field at $r = 9230\ km$, a location close to the crossover point between the O^+ and H^+ density profiles in the ambient polar wind. Before the heating, the normalized electric field at this location has a constant value of about 3.2. In response to the heating, the electric field is seen to undergo oscillations, which are sensitively controlled by the slope of the O^+ density profile because in our model $E = -(kT_o/e)n_e^{-1}\partial n_e/\partial x$, where $n_e = n_{O^+} + n_{H^+}$. From Figure 1 we noted that the crossover point between O^+ and H^+ density profiles is at $r \cong 9100\ km$. The heating occurs for $r > 8311\ km$. Near and below the crossover point, the O^+ density is significant compared to the H^+ density. Therefore any modulation in the O^+ density profile is reflected in the modulation of the electric field. Far above the crossover point, where $n_{O^+} << n_{H^+}$, the modulation in the O^+ density profile does not by itself cause a modulation in the electric field. However, the modulation in the electric field at relatively low altitudes does perturb the H^+ density resulting in some modulation in the electric field, even at high altitudes.

The inset of Figure 5 shows that in response to the heating, the electric field first sharply increases from its normalized value of 3.2 to 3.4 followed by a sharp drop and subsequent oscillations about a reduced level of time average electric field. These temporal features are related to the changes in the slope of the O^+ density profile. However, due to the log scale used in the density plots in Figure 5, it is difficult to clearly see the changes in the slope near $r \cong 9230\,km$. When plotted on a linear scale in a localized region, the density profiles do show the change in slopes as borne out from the oscillations in the electric field. The oscillations in the electric field modulate the outflow of the O^+ ions forming the bunches seen in Figure 4. Even a relatively small change in the electric field becomes significant in O^+ motion near the mirror points where the parallel velocity vanishes. In contrast, the H^+ flow is only slightly affected by the oscillations in the electric field because the flow is highly supersonic for most parts of the flux tube.

Oscillations in O^+ Density: The reformation of density expansion front in connection with the bounce motion of O^+ ions is found to cause well-defined periodic oscillations in the local densities. Figure 9 shows these oscillations in densities at some selected geocentric distances. The density oscillations at $r = 9270\,km$, where the O^+ density is large, is relatively weak. However at higher altitudes the relative amplitudes of the oscillations become quite appreciable. The first peak in the oscillations corresponds to the first wave of heated ions as they move upward under the influence of the mirror force. On the other hand, the subsequent peaks are the consequences of the passage of the expansion fronts. The sharpness of the increase in the densities is explained by the sharpness of the expansion fronts. The density at any altitude slowly decreases after the passage of the expansion front because as the plasma cloud expands, it occupies a larger volume giving rise to a progressively decreasing density. Note that the oscillation periods progressively increase with the increasing altitude. This simply implies that it takes longer for an expansion front to reach higher altitudes. Note that the oscillations occur up to distances of a few tens of thousands of kilometers.

takes longer for an expansion front to reach higher altitudes. Note that the oscillations occur up to distances of a few tens of thousands of kilometers.

The recurring reformation of the expansion front continues for a fairly long time until the superthermal ions disperse in altitude due to their different initial energies acquired during the heating period. We find that this time is about a day. The inset of Figure 10 shows the phase space plots of ions at $t = 24$ hrs. The ions are dispersed in altitudes up to $r \cong 29000$ *km*, where the apex of the trapped superthermal ions occur. The trapped ions are in a nearly diffusive equilibrium with average flow velocity approximately zero all along the flux tube. The density distribution associated with the phase space plots is also shown in Figure 10. For the purpose of comparison, we have also plotted the initial O^+ density profile just before the heating. The result of the heating is that the superthermal ions trapped in the flux tube significantly enhance the O^+ density up to altitudes of several thousands of kilometers. Such an enhancement may be part of the solution for the supply of O^+ ions to high altitudes where transverse ion heating produces energetic ions in *keV* energy range.

The phase space plots in Figure 10 reveals an interesting feature of the trapped O^+. The largest kinetic energy occurs near the bottom of the flux tube and it steadily decreases with altitude; near the apex the ions are super cold with an average energy less than that of the ambient O^+ ions in the ionosphere. Such cold ions may contribute to the hidden cold core, which are difficult to measure using particle detectors, but affect the characteristic plasma frequency. Such cold thermal O^+ ions have been observed up to altitudes of several thousand kilometers, and so far no explanation has been found as to how they reach such heights [*Abe et al*, 1993; *Peterson et al*, 1993]. Our study reveals that a low level of transverse ion heating at low altitudes in conjunction with the gravity creates a cold O^+ population extending to high altitudes.

The above features of O^+ produced by transverse heating occurs only for sufficiently low heating. For strong heating producing O^+ ions greatly in excess of 10 *eV* energy, most ions escape and the features discussed above become quite weak.

3.3 O^+ Flux

Outflux: In the past several studies have been performed on O^+ outflux [*Barakat and Schunk*, 1983; *Li et al*, 1988; *Korosmezey et al*, 1992; *Wilson*, 1993]. We show here that transverse ion heating lasting over a few minutes produces a time varying flux; the evolution of the flux as a function of altitude and time is examined here. For the low heating rate discussed in this paper, the evolution of outflux of O^+ at early times is shown in Figure 11a. In this figure we have plotted normalized outflux $\overline{\Gamma} = \overline{n}_{o+}\,\overline{u}_o\, r^3/(R_e + 1000\ km)^3$; the normalization factor $\Gamma_o = n_o V_{tH}$, which is $5{\cdot}5\times10^9\ ions\ cm^{-2}s^{-1}$, if we assume $n_o = 10^4\ cm^{-3}$ and $T_o = 0.3\ eV$.

We find that when the heating occurs at geometric distance $r > 8310\ km$ ($h > 1940\ km$), a large flux develops even below the heating region and it extends all the way down to the base at $r = r_b$, which has the height of 980 *km*. One minute after the heating begins, the maximum outflux at the base is $\Gamma = 6\times10^{-2}\,\Gamma_o$. If we assume $n_o = 10^4\ cm^{-3}$, and $T_o = 0.3\ eV$, $\Gamma_o = 5{\cdot}5\times10^9\ ions\ cm^{-2}s^{-1}$ and $\Gamma = 3\times10^8\ ions\ cm^{-2}s^{-1}$. This large flux develops due to average upward flow developing all the way down to the base. Figure 11b shows the evolution of the average flow velocity giving rise to the flux. At $t = 0$ the flow velocity is zero or less than zero all along the flux tube. At $t = 1$ min., the flow velocity at the base is $0.06\,V_{tH} \cong 324\ m/s$, and decreases with the increasing altitude. At later times, when the heated ions move upward, the flow velocity increases at higher altitudes while it decreases at lower altitudes and eventually it approaches zero there. This is illustrated by the curve for $t = 6$ min. in Figure 11b. It is interesting to examine how such a large flux develops at altitudes below the heating region. It is not due to any upward acceleration of ions below the heating altitude. Before the heating, downward and upward fluxes are nearly balanced giving a zero flux, but when heating occurs some downflowing ions in the initial population are not able to flow downward any more because of the mirror force. This creates an imbalance in favor of an upward flux.

Figures 12a and 12b show the further evolution of the outflux by plotting $\overline{\Gamma}$ at some selected times, at $t = 10$, 30 and 60 mins. in Fig. 12a and at $t = 2$, 3 and 4 hours in Fig. 12b. We see that as the outflux spreads upward its maximum value decreases; at

$t = 30$ min., $\Gamma_{max} \cong 2{\cdot}25 \times 10^{-3}\ \Gamma_o \cong 1{\cdot}2 \times 10^7\ ions\ cm^{-2}s^{-1}$ and for $t > 2$ hrs. the flux is less than $10^{-3}\Gamma_o \cong 5{\cdot}5 \times 10^6\ cm^{-2}s^{-1}$. The above values of the outflux should be compared against the flux produced by warm electrons, when electron temperature is enhanced from $3000°\,k$ to $10{,}000°\,k$ the outflux increases from a negligibly small value to $0{\cdot}4 \times 10^7\ ions\ cm^{-2}/s^{-1}$ [*Barakat and Schunk*, 1983]. A similar magnitude of flux in response to elevated O^+ temperature was reported by *Li et al* [1988]. We see that even a weak transverse ion heating can produce a substantially large flux extending to $r \sim 3 \times 10^4\ km$ in comparison to that produced by an enhancement in the electron and ion temperatures. However, the transverse heating, occurring over a brief time period of a few minutes, produces only a transient outflux. Figure 12b also shows that relatively weak outflux developing at relatively low altitudes at later times. For example, note the outflux below $r = 15{,}000\ km$ at all three times shown in the figure. Such fluxes are the consequences of secondary expansion fronts which develop when the down-flowing ions mirror upward. The pulse of flux just below $r = 15{,}000\ km$ at $t = 240$ min. corresponds to the expansion front shown by the arrow in Figure 4a. The three peak outfluxes for $r < 15{,}000\ km$ are approximately $5{\cdot}5 \times 10^6$, $1{\cdot}1 \times 10^6$, and $5{\cdot}5 \times 10^5\ ions\ cm^{-2}s^{-1}$ at $t = 2, 3$ and 4 hrs., respectively.

Downflux: From our previous discussion on down moving ions, we should expect downward fluxes developing in response to transverse ion heating. We discuss here the magnitude of the downward flux. We find two separate instances of downward flux. The first case occurs at very early stage of the heating and confined to quite low altitudes, even below the altitudes where heating occurs. The second case occurs after the upward moving ions are able to travel a substantial distance and then they are pulled down by the gravity.

Figure 13 shows the low-altitude downward flux occurring at early times. At $t = 10$ min., the maximum downward flux is $8 \times 10^{-3}\,\Gamma_o = 4{\cdot}4 \times 10^7\ ions\ cm^{-2}s^{-1}$ right near the base of the flux tube. How is this large downward flux created? In order to answer this question, we note from Figure 11a that a large upward flux develops at early time even at altitudes below the

heating. As noted earlier, this large outflux is due to the imbalance between the downward and upward flowing ions below the heating region caused by the heating of some of the downflowing ions at higher altitudes. This imbalance favoring upward flux does not last long. Since ions carrying the additional upward flux are not energized, they do not travel far and are turned downward by the gravity, creating a substantial downward flux at low altitude at an early time; for example, at $t = 10$ min. the downward flux is limited to altitude below the heating region for $r > 8310\ km$. At later time the downward flux is seen to penetrate into the heating region. This depends on the initial energies of the up-flowing ions carrying the upward unbalanced flux and the perpendicular energy they may receive in the heating region. If they receive relatively large perpendicular energy, they may not return and this reduces the downward flux as seen for $t = 30$ and 60 mins. in Fig. 13.

The large initial downward flux at low altitudes gives way to smaller downward flux when ions traveling to higher altitudes begin to return. Figure 14a shows such downward fluxes for $t = 2$, 3, and 4 hrs. In order to understand the downward flux, we have plotted the average flow velocity of O^+ in Figure 14b at the same times as in Figure 14a. At $t = 2$ hrs., we expect downward flux over the altitude range $10{,}000\ km < r < 19{,}000\ km$, for which the flow velocity $\bar{V} < 0$. We see the downward flux for this time in Figure 14a; the maximum flux occurs at about $r = 11{,}000\ km$ and its magnitude is $1{\cdot}6 \times 10^6\ ions\ cm^{-2}s^{-1}$. At later times the downward flux generally decreases, but it extends to higher altitudes, as we discussed earlier in connection with the phase space plots in Figures 3 and 4. We notice from Figure 14a that there are dropouts in the downward flux in some altitude intervals. Such dropouts occur at altitudes, where upward expanding density fronts are located at a given time. In the expansion front the flux is upward as shown in Figure 12b.

In view of Figure 14b, we may further amplify our discussion on the drift velocity of the downflowing ions. We notice that at times later than 2 hrs., after which expansion fronts begin to appear, the maximum downward drift velocity occurs just above the expansion front and the height where it occurs increases with increasing time. Furthermore, its magnitude increases with

the altitude. This increase in the magnitude of the maximum drift velocity is simply the consequence of the relatively more energetic ions traveling to higher heights and in the process of falling require a higher downward drift velocity.

4. Conclusion and Discussion

In this paper we have studied the time response of O^+ flow to a low level of transverse heating in the polar ionosphere. The heating is allowed to occur over a few minutes and the heating rate is kept sufficiently low so that the bulk of the heated ions have a few eV energies. Such ions do not escape the downward gravitational pull. Therefore, the heated ions first move upward as they are acted upon by the mirror force, but they are eventually turned downward by the gravity. While moving downward, the ions mirror back eventually and execute a bounce motion in the flux tube. The dynamics and the fluxes of O^+ associated with the initial upflow in response to the transverse heating and with the subsequent bounce motion are examined in this paper. The main results of this paper are as follows:

1) When a low level transverse ion heating occurs in the topside ionosphere, it generates a large outflow of O^+ even at altitudes below the heating region. This outflux is the consequence of the imbalance between the upward and downward fluxes. A large outflux below the heating region lasts over a few minutes, after which a large downward flux develops lasting again just over a few minutes. The interesting fact is that ions participating in such an event of large upward flux followed by a large downward flux below the heating region are generally unenergized.

2) The initial upward expansion of the heated ions significantly enhances O^+ density to geocentric distance up to several Re. However, the ions transported to high altitudes do not stay there. They are pulled down by the gravity. The height reached depends on the energy gained during the heating period. The lower the energy gain, the lower is the height reached

by the ions. Thus, during the course of the evolution of the heated ions it is possible to have up-flowing ions at high altitudes and down-flowing ions below them.

3) The average flow velocity of the down-flowing ions maximizes above the topside ionosphere because the dense cold plasma inside the ionosphere reduces the average velocity of the ions accelerating downward under the influence of the gravity even before the mirror force begins to dominate the gravity. The downward flow velocity of O^+ seen from the simulation is comparable to those observed from DE 1 [*Chandler*, 1995].

4) When downward flowing ions mirror back, they generate a series of expansion fronts moving upward from the ionosphere. The formation of such expansion fronts is seen to last over several hours in response to a brief heating time of just a few minutes. The width of the expansion front is determined by the heating time and the spread in the O^+ parallel velocity, which evolves due to the action of the mirror force and the gravity. Figure 6 shows that the expansion front is relatively thick at lower altitudes and becomes thinner as it moves upward because the O^+ ions progressively cool.

5) In response to the formation, and upward propagation of the expansion fronts, the local O^+ densities show nearly periodic oscillations with a time period increasing with altitude. The period ranges from about an hour at the topside ionosphere to several hours at the altitude of a few Re.

6) The formation of expansion fronts ceases when the heated ions, having a range of initial energies, disperse in space. This happens in about one day.

7) When the trapped heated ions have dispersed in space, the resulting O^+ density profile extends to large distances with significantly enhanced O^+ densities. Thus a low level transverse

heating occurring in the topside ionosphere is a possible mechanism for the supply of O^+ ion to the distant part of the magnetosphere.

8) When the trapped ions have dispersed in space, the ions with largest kinetic energies occur in the topside ionosphere, while the coldest ions with energies less than the characteristic ionospheric energy (kT_o) occur at large geocentric distances near the apex of the trapped ion trajectories. Thus a low-altitude heating is a mechanism for producing the cold plasma population. Such populations are difficult to measure by particle detectors while they affect the plasma frequency. This yields a higher estimate of plasma density from wave measurements compared to that from direct particle measurements. However, cold thermal ions have been observed at distances of several tens of thousand of kilometers from DE-1 [*Abe et al*, 1993; *Peterson*, 1993], but without a plausible explanation. Our study here provides a plausible explanation in terms of a low level transverse heating in the topside ionosphere in conjunction with the downward gravitational force, which reduces the kinetic energy as the ions travel to higher altitudes.

9) Simulation predicts a range of fluxes for both up- and down-flowing ions. The O^+ outfluxes resulting from the transverse heating are generally transient. The maximum magnitude of such outfluxes is about $\sim 10^7 ions\ cm^{-2}s^{-1}$, as predicted by previous steady-state models [*Barakat and Schunk*, 1983; *Li et al*, 1988]. In addition to the upward flux of the heated ions, a transient heating event causes a relatively large transient outflux of O^+ ions below the heating region. This is simply caused by the imbalance in the upward and downward fluxes when the downward flowing ions mirror back due to the transverse heating.

10) Except for a large downward flux during the early stage of the heating at low altitudes below the heating region, the downward flux of O^+ above the dense O^+ plasma is found to be

$\sim 10^6$ *ions* $cm^{-2}s^{-1}$. The downward drift and flux show a great deal of variability with both time and altitude.

Finally, we point out that in the one-dimensional calculations presented here, the convection electric field was ignored. Therefore, the results presented here are the response of a single flux tube as it convects, keeping all its plasma contents as under the frozen-in-field approximation. In other words, an observer moving with the convecting flux tube should see the processes described here. In the rest frame of reference, the inclusion of the convection electric field gives rise to a hopping motion as revealed by a two-dimensional trajectory calculation of *Horwitz* [1984]. In order to assess the influence of the hopping motion on the dynamical behavior of the superthermal O^+ ions, a two-dimensional model based on self-consistent electric field is needed. However, for a heating region extending both in longitude and latitude, the results presented here should be qualitatively applicable; in such a situation the rising and falling ions should uniformly repeat themselves. The most important result of this paper on the creation of a cold O^+ population at high altitudes should not be modified by the convection electric field. A multitude of heating events randomly distributed in space and time should produce the cold O^+ ion population at altitudes up to several thousand kilometers in a large volume of space covering the polar and auroral regions.

Acknowledgment: This work was performed under the NASA grant NAGW-2903.

References

Abe, T., B. A. Whalen, A. W. Yau, R. E. Horita, S. Watanabe, and E. Sagawa, EXOS D (Akebono) superthermal mass spectrometer observations of the polar wind, *J. Geophys. Res.*, *98*, 11,191, 1993.

Barakat, A. R., and R. W. Schunk, O^+ ions in the polar wind, *J. Geophys. Res.*, *88*, 7887, 1983.

Barakat, A. R., R. W. Schunk, and J.-P. St. Maurice, Monte Carlo calculations of the O^+ velocity distribution in the auroral ionosphere, *J. Geophys. Res.*, *88*, 3237, 1983.

Brown, D. G., G. R. Wilson, J. L. Horwitz, and D. L. Gallagher, Self-consistent productions of ion conics on return current region auroral field lines: A time-dependent, semi-kinetic model, *Geophys. Res. Lett.*, *18*, 1841,1991.

Chandler, M. O., Observations of downward moving O^+ in the polar topside ionosphere, *J. Geophys. Res.*, *100*, 5795, 1995.

Gombosi, T. I., and T. L. Killeen, Effects of thermospheric motions on the polar wind: A time-dependent numerical study, *J. Geophys. Res.*, *92*, 4725, 1984.

Horwitz, J. L., Parabolic heavy ion flow in the polar magnetosphere, *J. Geophys. Res.*, *92*, 175, 1984.

Horwitz, J. L., and M. Lockwood, The cleft ion fountain: A two-dimensional kinetic model, *J. Geophys. Res.*, *90*, 9749, 1985.

Korosmezey, A., C. E. Rasmussen, T. I. Gombosi, and G. V. Khazanov, Anisotropic ion heating and parallel O^+ acceleration in regions of rapid $\underline{E} \times \underline{B}$ convection, *Geophys. Res. Lett.*, *19*, 2289, 1992.

Li, Peng, G. R. Wilson, and J. L. Horwitz, Effect of mid-altitude ion heating on ion outflow at polar latitudes, *J. Geophys. Res.*, *93*, 9753, 1988.

Lockwood, M., M. O. Chandler, J. L. Horwitz, J. H. Waite, Jr., T. E. Moore, and C. R. Chappell, The cleft ion fountain, *J. Geophys. Res.*, *90*, 9736, 1985.

Loranc, M., and J.-P. St.-Maurice, A time-dependent gyro-kinetic model of thermal ion upflows in the high-altitude $\underline{F}$ region, *J. Geophys. Res.*, *99*, 17,429, 1994.

Peterson, W. K., A. W. Yau, and B. A. Whalen, Simultaneous observations of H^+ and O^+ ions at two altitudes by the Akebono and Dynamic Explorer 1 satellites, *J. Geophys. Res.*, *98*, 11,177, 1993.

Schunk, R. W., and J. L. Sojka, A three-dimensional time-dependent model of the polar wind, *J. Geophys. Res.*, *94*, 8973, 1989.

Singh, N., K. S. Hwang, D. G. Torr, and P. Richards, Temporal features of the outflow of heavy ionospheric ions in response to a high altitude plasma cavity, *Geophys. Res. Lett.*, *16*, 29, 1989.

Waite, J. H., Jr., T. Nagai, J. F. E. Johnson, C. R. Chappell, J. L. Burch, T. L. Killeen, P. B. Hays, G. R. Carrigan, W. K. Peterson, and E. G. Shelley, Escape of superthermal O^+ ions in the polar cap, *J. Geophys. Res.*, *90*, 1619, 1985.

Wilson, G. R., Kinetic modeling of O^+ upflows resulting from $\underline{E} \times \underline{B}$ convection heating in the high-altitude $\underline{F}$ region, *J. Geophys. Res.*, *99*, 17,453, 1994.

Wilson, G. R., C. W. Ho, J. L. Horwitz, N. Singh, and T. E. Moore, A new kinetic model for time-dependent polar plasma outflow: Initial results, *Geophys. Res. Lett.*, *17*, 263, 1990.

FIGURE CAPTIONS

Fig. 1. Geometry of the flux tube. We consider a flux tube from a geocentric distance r_b to r_{max}. In the simulation macroparticles representing O^+ and H^+ ions are injected into the flux tube at the base $r = r_b$ and those exiting the flux tube at $r = r_{max}$ are assumed to be lost.

Fig. 2. The properties of the ambient polar wind ($t = 0$). (a)-(b) Phase space plots of O^+ ions. (c)-(d) Phase space plots for H^+ ions. Left and right hand panels for the phase space plots are in $r - V_{\parallel}$ and $r - V_{\perp}$ planes, respectively. Each dot in the phase space represents a macro O^+ or H^+ ion. (e) O^+ and H^+ density, and electric field profiles. (f) O^+ and H^+ average flow velocities and H^+ outflux $\overline{\Gamma}$.

Fig. 3. Same as Figure 2, but for later times. (a)-(b) $t = 5$ min., (c)-(d) $t = 20$ min., (e)-(f) $t = 60$ min., and (g)-(h) $t = 120$ min. Note that at $t = 120$ min., both down and upflowing ions occur.

Fig. 4. Same as Figure 3, but for later times. (a) - (b) $t = 4$ hrs., (c) - (d) $t = 6$ hrs., (e) - (f) $t = 8$ hrs., and (g) - (h) $t = 12$ hrs. Note the rising O^+ clouds as indicated by arrows.

Fig. 5. Density profiles during the initial upward expansion of the heated ions. The solid-line curve shows the O^+ density profile for the ambient polar wind ($t = 0$). Note the beginning of re-expansion at $t = 180$ min. The inset shows the temporal evolution of the electric field at $r = 9230$ *km*.

Fig. 6. Same as Fig. 5, but for later times showing further motion of the expansion front appearing at $t = 180$ min. Note a new expansion front appearing at $t = 360$ min.

Fig. 7. Average flow velocity associated with the expansion front shown in Figure 6.

Fig. 8. Further upward motion of the new expansion front at $t = 360$ min., as noted in Fig. 6. The new expansion front, indicated by short arrows, has reached $r \cong 16{,}000$ *km* at $t = 8$ hrs. The old expansion front (indicated by long arrows) has reached $r \cong 23{,}00$ *km* at the same time.

Fig. 9. Characteristic density oscillations at some selected geocentric distances in response to the formation and propagation of fronts shown in Figs. 6 to 8.

Fig. 10. Density profile associated with the trapped superthermal ions at $t = 24$ hrs. The initial density profile without the heating is also shown. Note the enhancement in the density for $r > 10{,}000$ *km*. The inset shows the phase-space plots for the diffused superthermal ions trapped inside the flux tube. Note that the warmest population of O^+ occurs near the bottom of the flux tube, while near the apex of the trapped O^+ ions are quite cold.

Fig. 11. (a) Outflux at early times, and (b) average flow velocity associated with the outflux in (a).

Fig. 12. Outflux at times later than were shown in Figure 11a: (a) Fluxes at $t = 10$, 30 and 60 mins., and (b) Fluxes at $t = 2$, 3 and 4 hrs. Note the "pulse" of outflux developing for $r < 15{,}000$ *km*; the flux is generated by the expansion fronts shown in Figure 6.

Fig. 13. Downward flux at relatively early times.

Fig. 14. (a) Downward flux at times later than those shown in Figure 13, and (b) average flow velocity associated with the downward flux in (a).

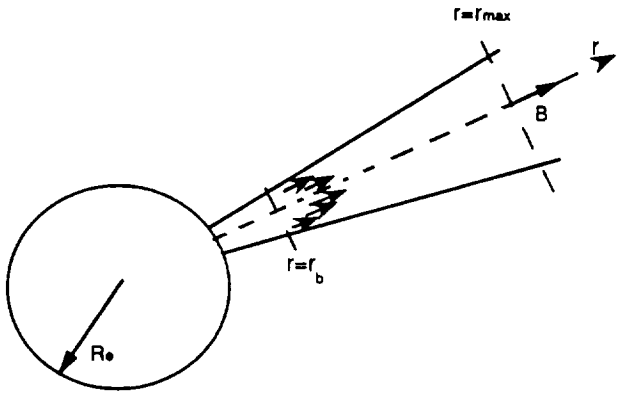

Fig. 1

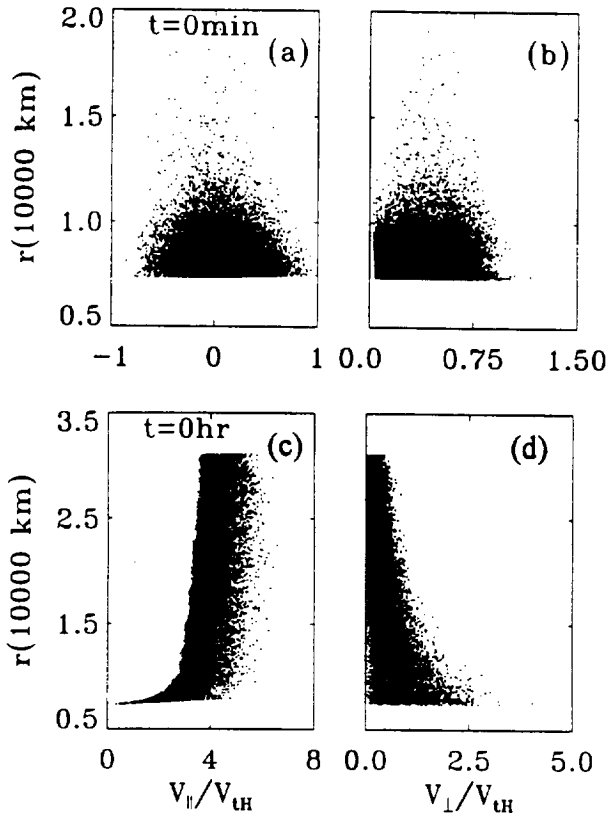
t=0min
(a)
(b)
2.0
1.5
1.0
0.5
r(10000 km)
−1
0
1
0.0
0.75
1.50
t=0hr
(c)
(d)
3.5
2.5
1.5
0.5
r(10000 km)
0
4
8
0.0
2.5
5.0
$V_{\parallel}/V_{tH}$
$V_{\perp}/V_{tH}$

Fig. 2

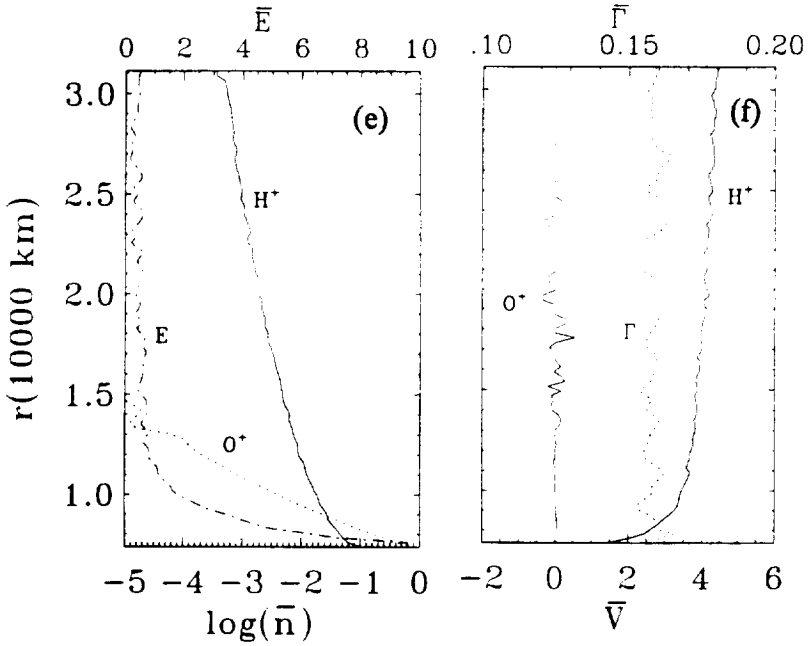

Fig. 2 Continued

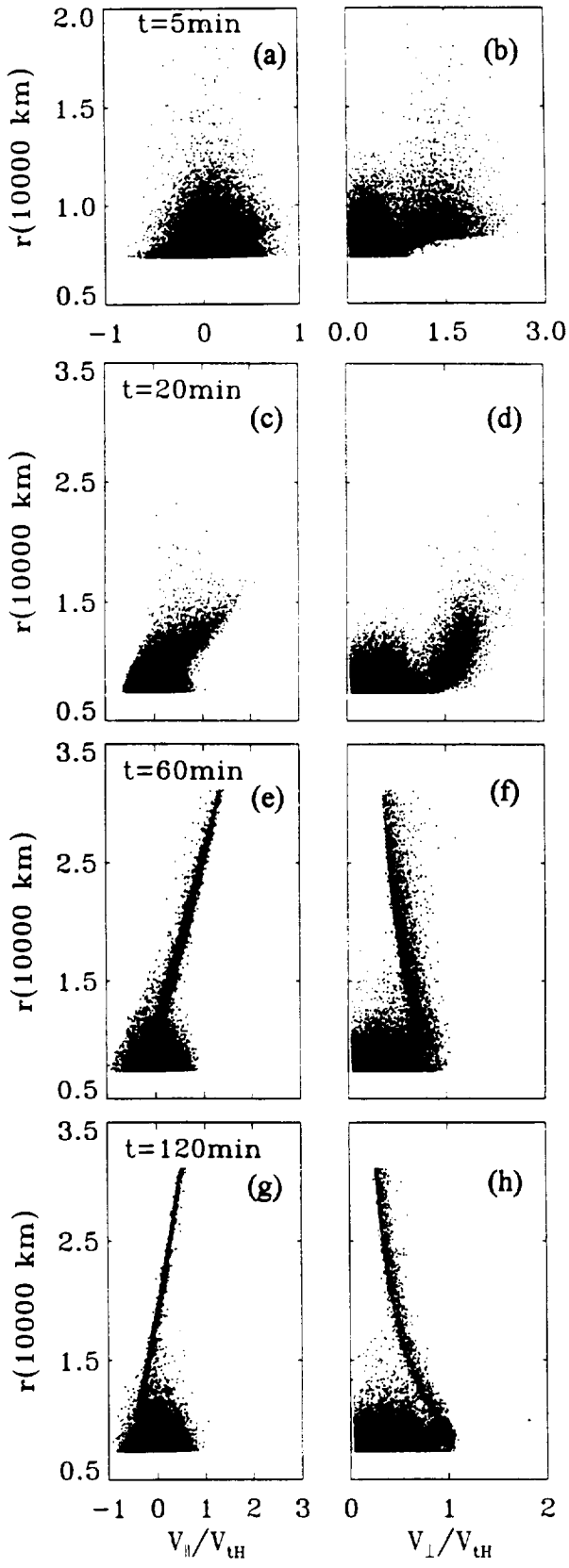
t=5min
(a)
(b)
t=20min
(c)
(d)
t=60min
(e)
(f)
t=120min
(g)
(h)
r(10000 km)
2.0
1.5
1.0
0.5
3.5
2.5
1.5
0.5
−1
0
1
0.0
1.5
3.0
2
3
$V_{\parallel}/V_{tH}$
$V_{\perp}/V_{tH}$

Fig. 3

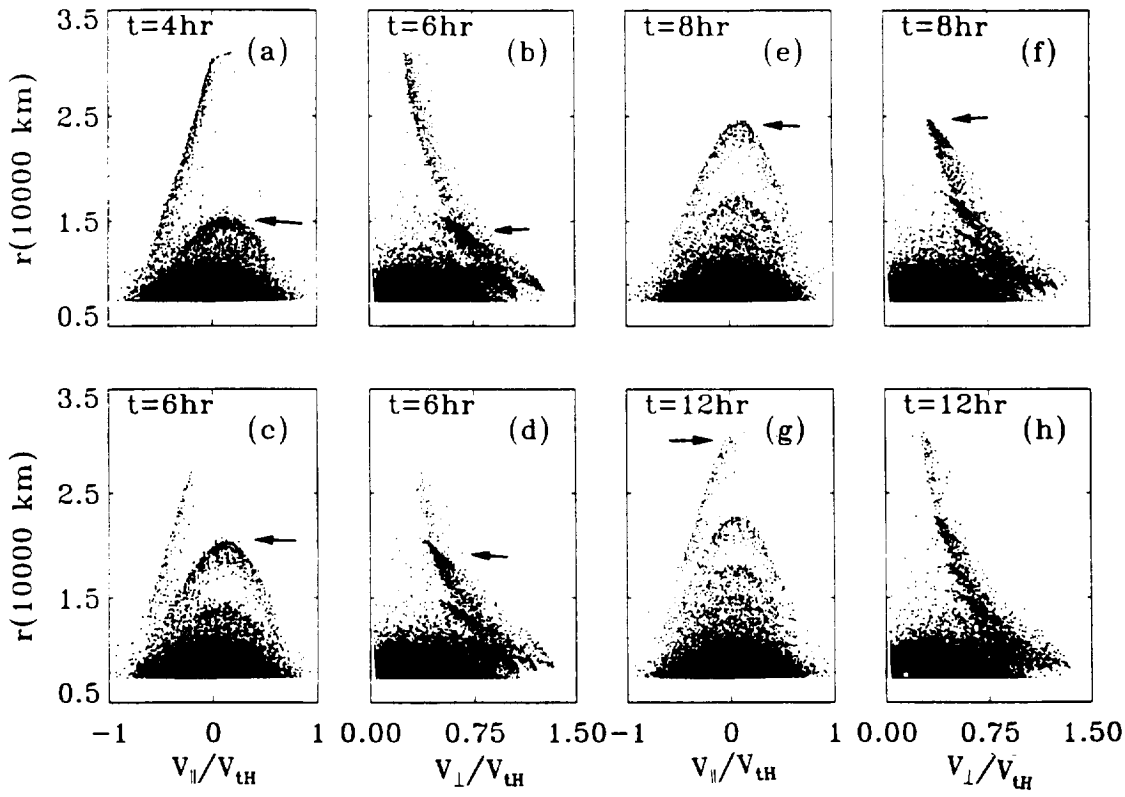
t=4hr
(a)
t=6hr
(b)
t=8hr
(e)
t=8hr
(f)
t=6hr
(c)
t=6hr
(d)
t=12hr
(g)
t=12hr
(h)
r(10000 km)
3.5
2.5
1.5
0.5
−1
0
1
0.00
0.75
1.50
$V_{\parallel}/V_{tH}$
$V_{\perp}/V_{tH}$

Fig. 4

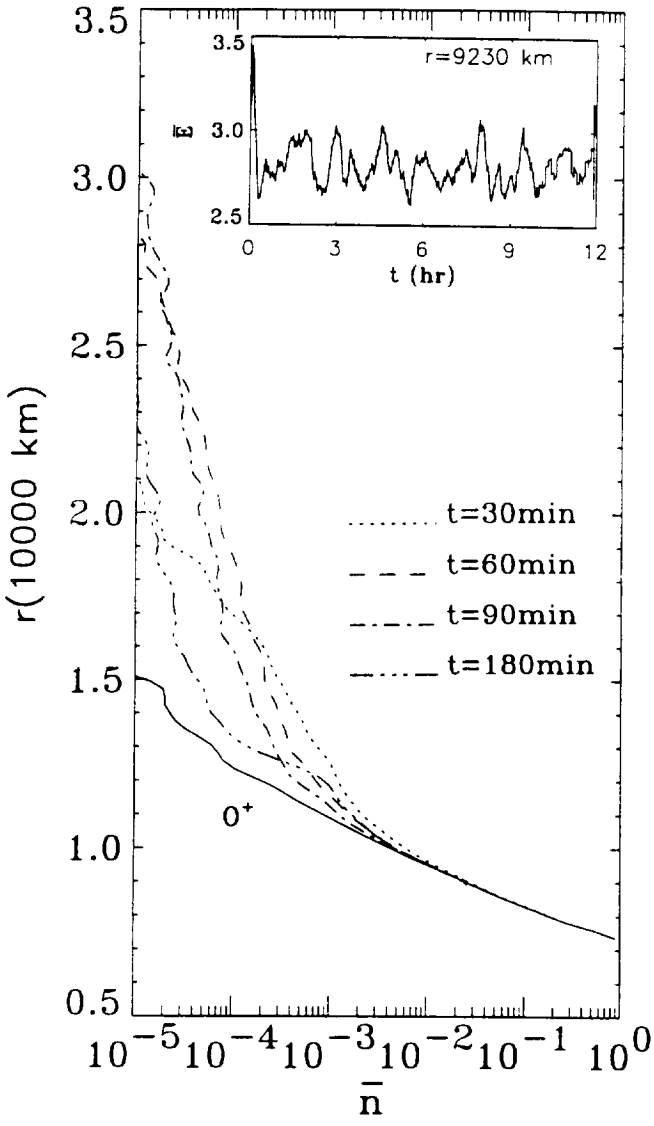

Fig. 5

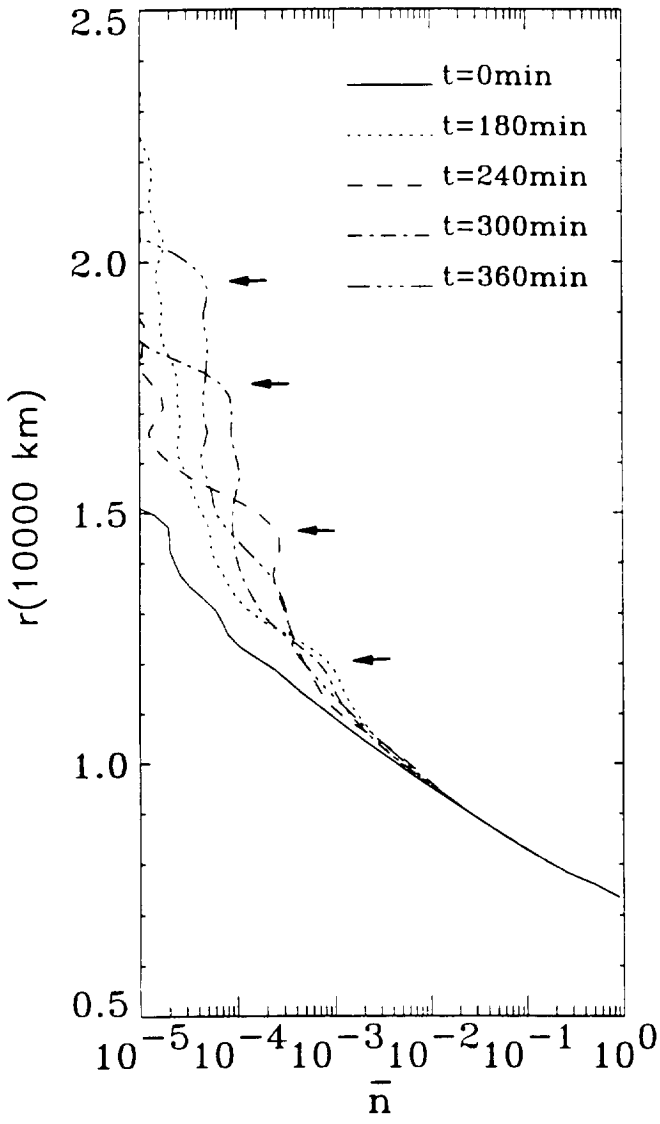
2.5
2.0
1.5
1.0
0.5
r(10000 km)
t=0min
t=180min
t=240min
t=300min
t=360min
10^{-5} 10^{-4} 10^{-3} 10^{-2} 10^{-1} 10^{0}
$\bar{n}$

Fig. 6

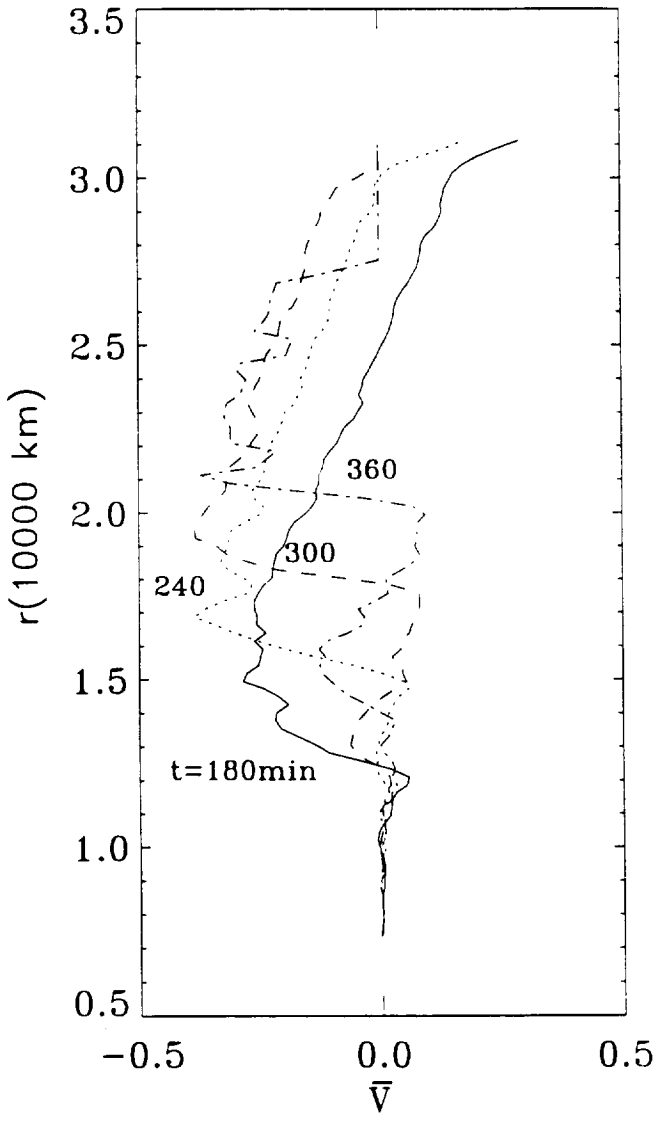

Fig. 7

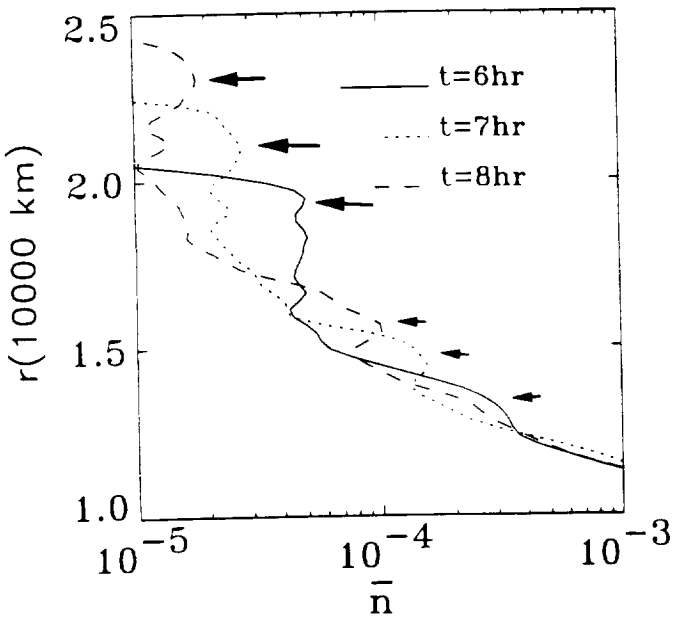

Fig. 8

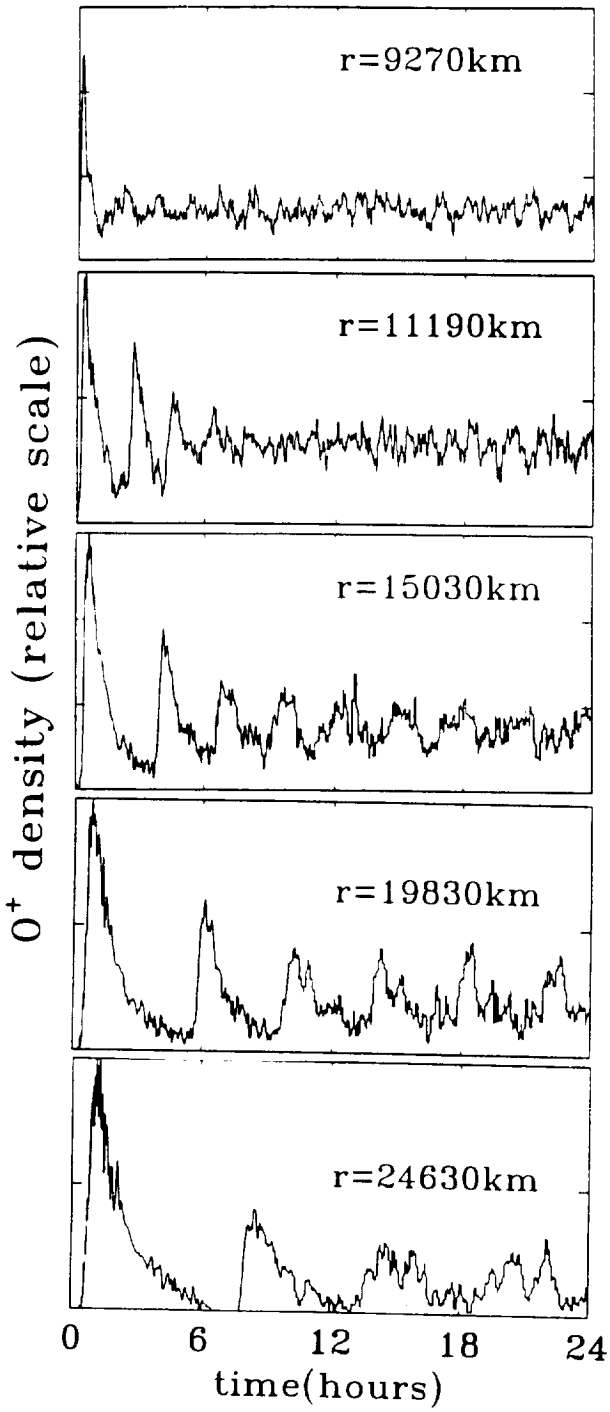
r=9270km
r=11190km
r=15030km
r=19830km
r=24630km
O+ density (relative scale)
0
6
12
18
24
time(hours)

Fig.9

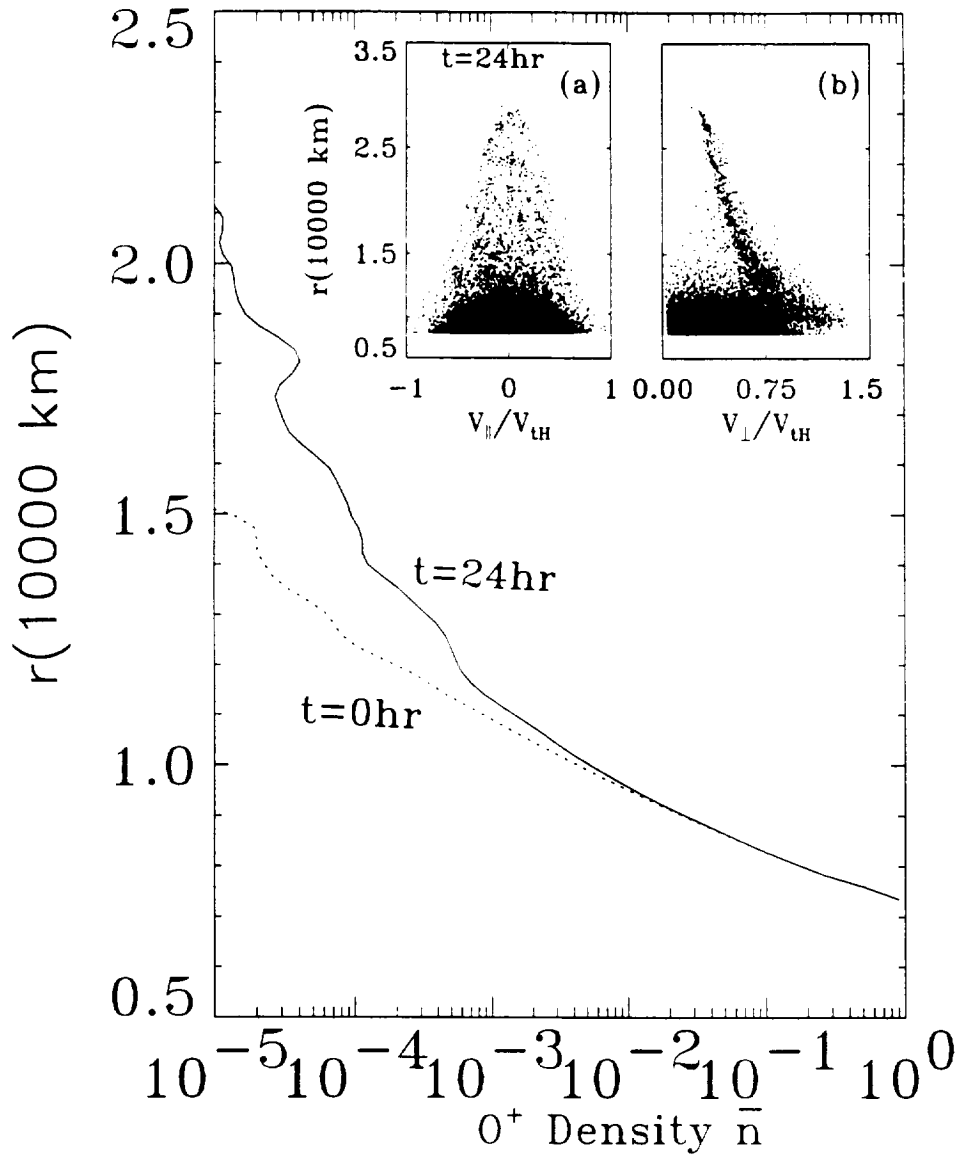
2.5
2.0
1.5
1.0
0.5
r(10000 km)
t=24hr
t=0hr
3.5
2.5
1.5
0.5
r(10000 km)
t=24hr
(a)
(b)
−1
0
1
0.00
0.75
1.5
$V_{\parallel}/V_{tH}$
$V_{\perp}/V_{tH}$
10^{-5} 10^{-4} 10^{-3} 10^{-2} 10^{-1} 10^{0}
O^{+} Density $\bar{n}$

Fig. 10

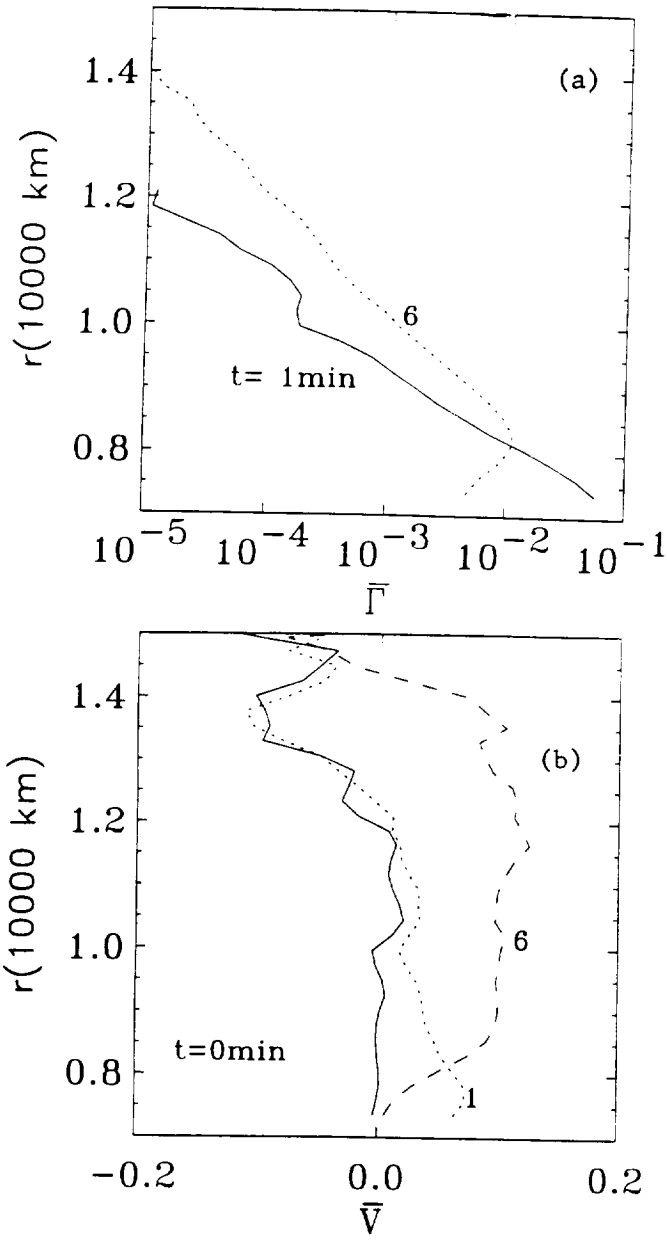
(a)
1.4
1.2
1.0
0.8
r(10000 km)
6
t= 1min
10^{-5} 10^{-4} 10^{-3} 10^{-2} 10^{-1}
$\bar{\Gamma}$
(b)
1.4
1.2
1.0
0.8
r(10000 km)
6
1
t=0min
−0.2
0.0
0.2
$\bar{V}$

Fig. 11

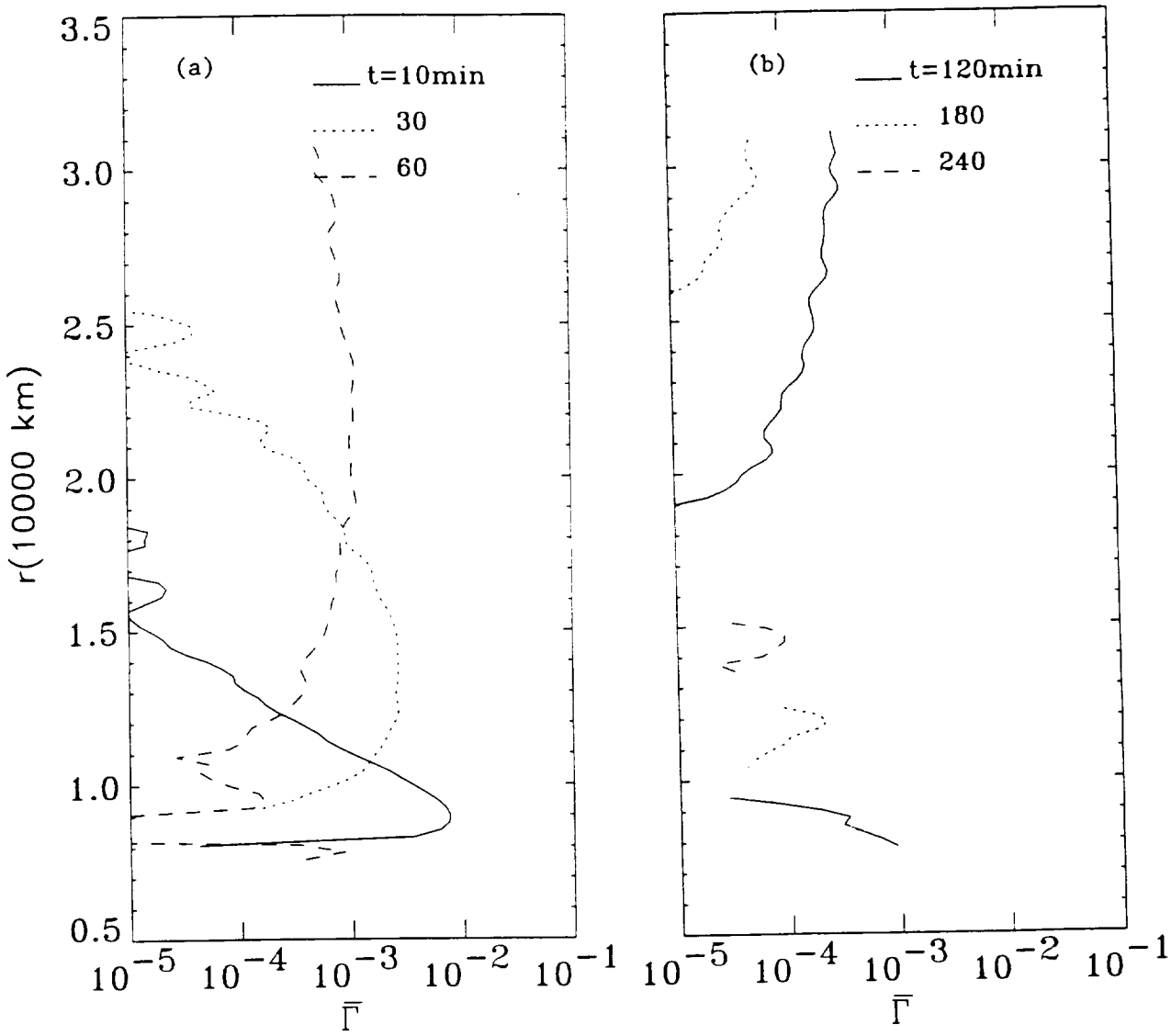
(a)
t=10min
30
60
(b)
t=120min
180
240
r(10000 km)
3.5
3.0
2.5
2.0
1.5
1.0
0.5
10^{-5} 10^{-4} 10^{-3} 10^{-2} 10^{-1}
$\bar{\Gamma}$

Fig. 12

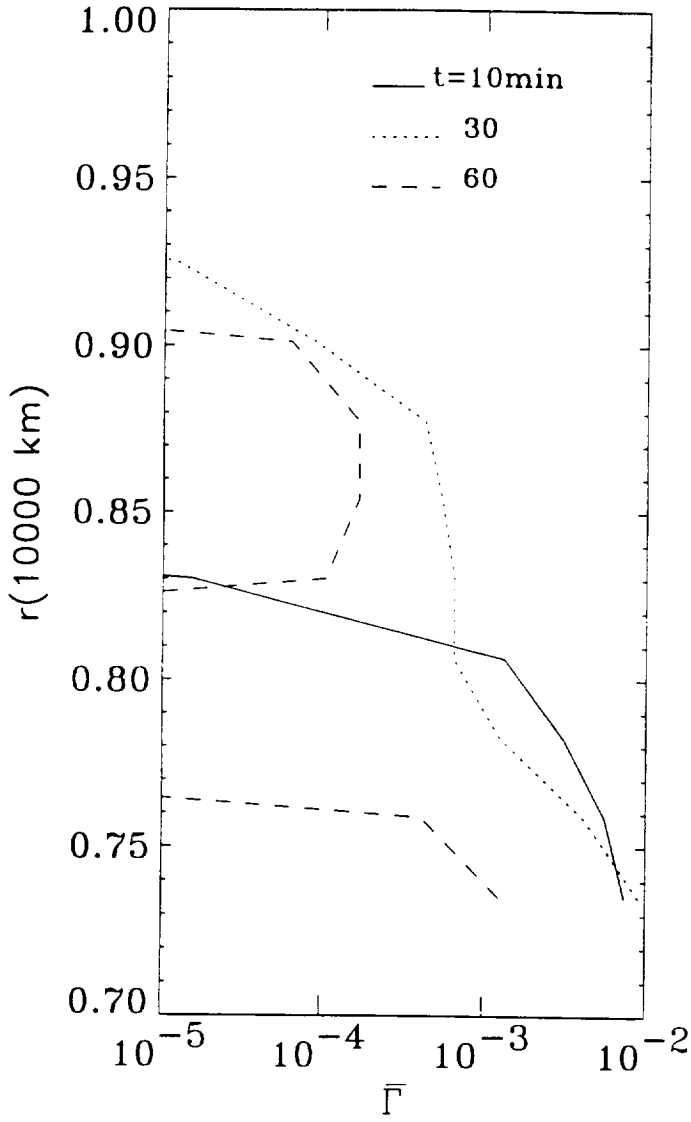
1.00
0.95
0.90
0.85
0.80
0.75
0.70
r(10000 km)
t=10min
30
60
10^{-5}
10^{-4}
10^{-3}
10^{-2}
$\bar{\Gamma}$

Fig. 13

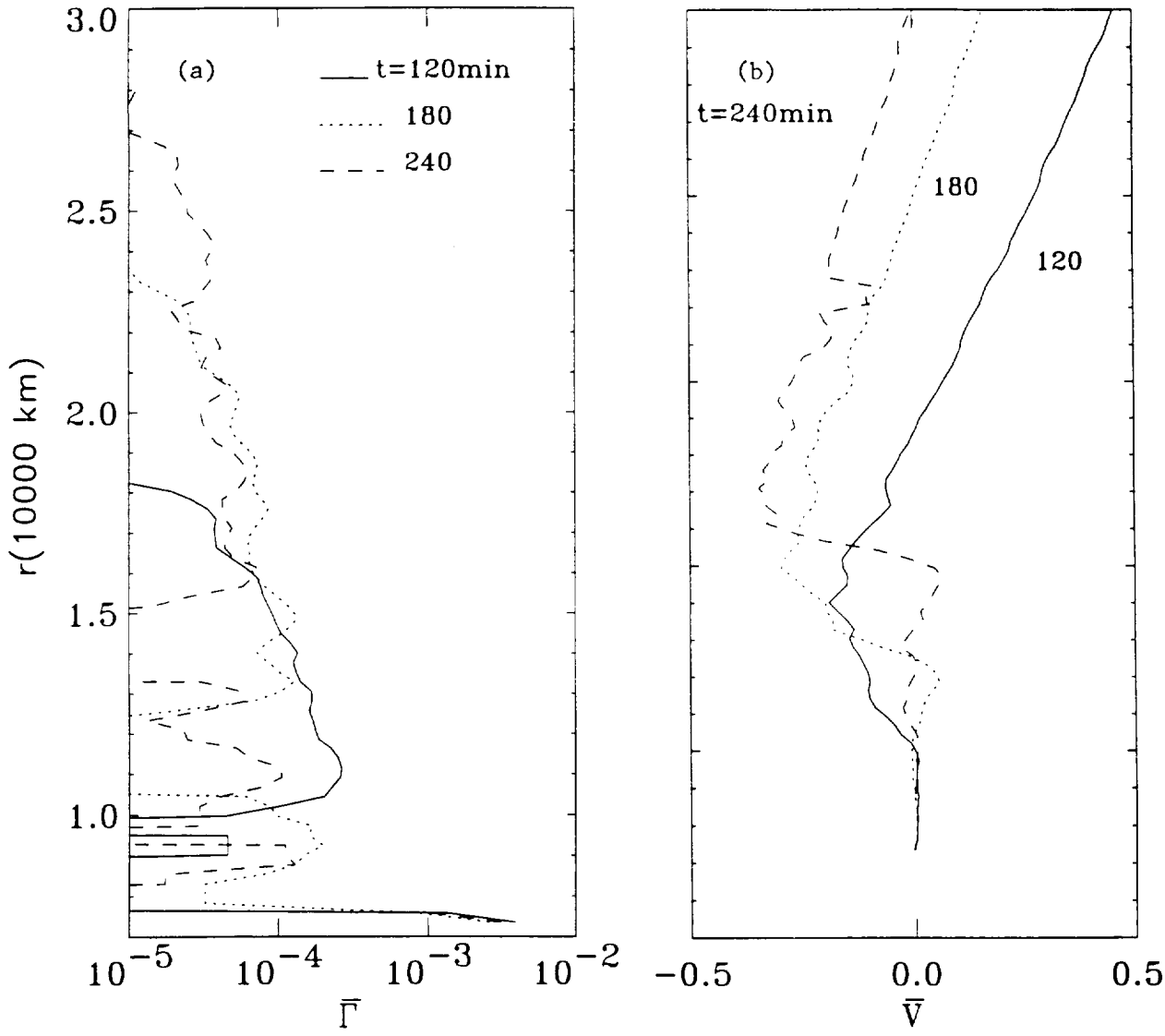
(a)
t=120min
180
240
3.0
2.5
2.0
1.5
1.0
r(10000 km)
10^{-5}
10^{-4}
10^{-3}
10^{-2}
$\bar{\Gamma}$
(b)
t=240min
180
120
-0.5
0.0
0.5
$\bar{V}$

Fig.14

Fountain-Like Flow of Heavy Oxygen Ions From the Earth's Ionosphere in Response to Transverse Heating

Nagendra Singh
Department of Electrical and Computer Engineering
University of Alabama in Huntsville, Huntsville, AL 35899

Abstract:

Normally the gravitationally bound heavy O^+ ions in the Earth's ionosphere are in a diffusive equilibrium. However, when energized to superthermal energies of a few *eV* transverse to the geomagnetic field, the combined effects of the downward gravitational and the upward electric and mirror forces produce interesting flow patterns in the vertical direction like in a pulsating fountain. This flow pattern is studied by means of a particle-in-cell code.

It is well known that the topside ionosphere is commonly populated with a variety of ion species such as H^+, O^+, and H_e^+. The light ions (H^+ and H_e^+) readily escape the downward gravitational force even when they have a small characteristic energy of about a few tenths of an *eV*. On the other hand, for the heavy O^+ ions the escape requires some sort of energization. For example, an O^+ ion escapes when its energy $W > W_{es} \cong m_{O^+} g_o R_e^2 / r$, where m_{O^+} is O^+ mass, g_o is the Earth's gravity at its surface, R_e is the Earth's radius, and r is the geocentric distance in the topside ionosphere. Using $R_e \cong 6371\ km$, $g_o = 9.8\ ms^{-2}$ and $r \cong 7350\ km$, the escape energy $W_{es} \cong 7.5\ eV$. For $W < W_{es}$ the O^+ ions can be transported to large altitudes, but they eventually fall down. If the energization occurs in the degree of freedom parallel to the magnetic field, the falling ions are lost into the ionosphere. On the other hand, when the heating occurs in the degree of freedom transverse to the geomagnetic field, the O^+ ions are trapped in the flux tube and undergo a bounce motion under the influence of the downward gravitational force and the upward mirror force associated with the downward gradient in the geomagnetic field $\underline{B}$. The upward polarization electric field associated with the density gradient also plays a critical role in the bounce motion.

We study vertical plasma flow in geomagnetic open flux tubes, which are typical of the polar ionosphere. The topside ionospheric base is assumed to be at $r = r_b \cong 7350\ km$. We simulate the flux tube from $r = r_b$ to a geocentric distance $r = r_{max} = 31{,}350\ km$. In order to study the plasma flow, we employ a particle code [1]. We inject macroparticles corresponding to O^+ and H^+ ions into the flux tube at the boundary at $r = r_b$ and subsequently follow their dynamics under the influence of the gravity, polarization electric field and the mirror force associated with the gradient in the geomagnetic field. The injected particles are chosen from Maxwellian velocity distributions with a zero drift for O^+ and a drift of $2V_{th}$ for H^+, where V_{th} is the thermal velocity corresponding to the temperature T_o of H^+ ions at the base. We assume that O^+ and electron temperatures at $r = r_b$ are also T_o. When a steady-state polar wind flow is set up in the flux tube, we initiate the transverse heating event for O^+ ions at geocentric distances $r \geq 8311\ km$. The heating at such altitudes is expected to be caused by wave-particle interactions and it is incorporated in a random fashion as described by Brown et al [2]. We present here the flow pattern of O^+ ions. The H^+ ions do not show any interesting feature except for their supersonic escape. Since H_e^+ ions have extremely low concentration compared to that of O^+ and H^+, they are not included in the model.

We show the bounce motion of the heated ions and its temporal evolution through a sequence of phase space plots after a brief heating event of 5 minutes at an average rate of about $0.04\ kT_o / s$. When $kT_o \cong 0.3\ eV$, this leads to a maximum energization of about $15\ eV$. Therefore, some of the ions, having energies $W > W_{es}$ escape while those with $W < W_{es}$ are trapped. Figs. 2a, 2b and 2c show the initial diffusive state of the O^+. Note that the left, middle and right panels in Fig. 1 are the phase space plots in $r - V_{\parallel}$, $r - V_{\perp}$ and $r - W$ planes, where r is the geocentric vertical distance, $V_{\parallel}$ and $V_{\perp}$ are the O^+ velocity components parallel and perpendicular to the geomagnetic field line, respectively, and $W = \frac{1}{2} m_o (V_{\parallel}^2 + V_{\perp}^2)$, that is, it is the total kinetic energy. Each dot in the figures represent an O^+ ion. Figures 2a, 2b and 2c show that the bulk of O^+ ions are generally confined below an altitude $r \cong 10^4\ km$.

The state of the O^+ flow after 6 hours of the brief heating period is shown in Figs 2d, 2e and 2f. Note that some ions have reached near the top of the simulated flux tube and have $V_{\|} > 0$, implying that they will escape. While those having $V_{\|} < 0$ are falling. Those ions are transported to high altitudes by the mirror force $F_m \propto -\frac{1}{2} m_o V_{\perp}^2 B^{-1} (\partial B / \partial r)$. The transverse heating increases $V_{\perp}$ and enables the upward flow. But the gravity pulls them downward if they do not have sufficiently large energy to escape.

The falling ions mirror back and expand upward and they appear in clumps; the clumps are seen in the form of evolving bands in the $r - V_{\|}$ plane as seen from Figs 2d, 2g, and 2j. The bands give the appearance of a water fountain. The bands can be seen as clusters of ions in the $r - V_{\perp}$ plane. $V_{\perp}$ decreases with increasing r due to the conservation of the magnetic moment $\mu = \frac{1}{2} m V_{\perp}^2 / B$. In terms of energy, the ion clusters appear in the form of "bananas," which simply manifest that the upgoing ions have slightly more kinetic energy than the downflowing ions. In both $r - V_{\perp}$ and $r - W$ planes, the upflowing $(V_{\|} > 0)$ ions are shown in green while the downflowing are shown in blue.

The cluster formation occurs by the modulation in the electric field E due to the falling and rising O^+ ions because E depends on the density gradients. This modulation of E also causes the difference in the kinetic energies of the upgoing and downgoing ions in any given cluster.

Acknowledgment: This work was performed under the grant NAGW-2903.

References

[1] G. R. Wilson, C. W. Ho, J. L. Horwitz, N. Singh, and T. E. Moore, *Geophys. Res. Lett., 17*, 263, 1990.

[2] D. G. Brown, G. R. Wilson, J. L. Horwitz, and D. Gallagher, *Geophys. Res. Lett., 18*, 1841, 1991.

Figure Captions

Fig. 1. Phase space plots in $r-V_{\parallel}$ (left panels), $r-V_{\perp}$ (middle panels), and $r-W$ (right panels) at several times are shown. Note that the velocity components are normalized with respect to the thermal velocity of H^+ ions which is about $5.4\ km/s$ for $kT_o = 0.3\ eV$ and energy is normalized in terms of kT_o. In the middle and right panels, blue represents falling O^+ ions, while green represents upflowing ones.